Atomic Structure of Amorphous Silicon Nitride Fibers

K. W. R. Gilkes
School of Physics, University of East Anglia, Norwich, U.K.

The atomic structure of amorphous silicon nitride fibers produced by two different methods is revealed using the technique of neutron scattering. Polymer-derived fibers are found to contain excess crystalline silicon and disordered carbon, and fibers annealed in N_2 for 100 h contain a cristobalite phase that becomes amorphous under 200-kV electron irradiation. Fibers grown from the gas phase, however, are shown to consist of almost pure amorphous Si_3N_4, with a small crystalline α-Si_3N_4 component.

Introduction

The development of new techniques for the synthesis of nonoxide ceramic fibers has been fueled by the need for high tensile strength fibers capable of use in oxidizing environments at temperatures up to 1,400°C. The lifetime of commercially available silicon carbide fibers is limited above 1,000°C, as they undergo structural changes in this temperature range. Silicon nitride, however, is stable at temperatures exceeding 1,400°C, and should therefore be a good candidate for high-temperature applications.

The fibers studied in this work were produced at Dow Corning, (Michigan) and the Swiss Federal Laboratories for Materials Testing and Research (EMPA) (Dubendorf, Switzerland). Researchers at Dow Corning used pyrolysis of a polymer precursor (hydridopolysilazane) to obtain continuous fibers with diameters greater than 10 μm. These fibers possess a tensile strength of up to 3 GPa and an elastic modulus of 260 GPa (Legrow et al., 1987). The fibers have a typical composition of $Si_{0.41}N_{0.39}C_{0.16}O_{0.04}$. ^{29}Si nuclear magnetic resonance (NMR) spectroscopy has been performed on the fibers, and suggests the possibility of bonding between Si and C, N, and O in the fibers (Legrow et al., 1987; Lipowitz, 1991). In addition, excess free carbon has been observed in HPZ fibers using transmission electron microscopy (TEM) and Raman spectroscopy (see Lipowitz, 1991).

Researchers in the high-performance ceramics group at EMPA have used a gas-phase process to grow both amorphous and crystalline silicon nitride fibers from silica powder through the decomposition of ammonia at temperatures between 1,400 and 1,500°C (Vogt et al., 1995). Amorphous fibers with tensile strengths as high as 5 GPa have been grown, and show no crystallization or other structural modifications when annealed below 1,400°C in argon, or 1,500°C in nitrogen (Chollon et al., 1996). Annealing in air, however, results in oxidation of the fiber surface at temperatures above 1,200°C (Vogt et al., 1996). ^{29}Si NMR spectroscopy has been used to characterize the amorphous fibers, and indicates the presence of an amorphous nonstoichiometric silicon oxynitride phase $Si_3N_{4-x}O_{1.5x}$ in addition to Si_3N_4 (Vogt et al., 1995).

The purpose of this study is to characterize and compare the atomic structure of the amorphous fibers produced by the two different methods described above. While ^{29}Si NMR spectroscopy gives useful information on the chemical species present in the sample, the long relaxation times necessary to achieve quantitative information limit the usefulness of the technique for noncrystalline samples. Neutron scattering, on the other hand, can provide detailed quantitative information on the local atomic environment in amorphous materials, as expressed by the bond lengths, bond angles, and coordination numbers. These structural parameters can be used to model the local *positional* (as opposed to chemical) order in the material, and therefore provides complementary information to NMR.

Experimental

Three amorphous fiber samples have been used for neutron scattering measurements. The first two are polymer-derived fibers produced by Dow Corning. The first is in the as-prepared state, and the second has been annealed at 1,400°C in a nitrogen atmosphere for 100 h, in order to assess its structural stability at high temperatures. These samples will be referred to as HPZ1 and HPZ2, respectively. The third sample has been produced by U. Vogt and coworkers at EMPA using the gas-phase process described earlier, and will be denoted EMPA.

Neutron scattering measurements were performed at the ISIS facility of the Rutherford Laboratory, Oxfordshire, UK, using the liquids and amorphous solids diffractometer (LAD). All three samples were powdered and loaded into thin-walled vanadium cans for insertion into the neutron beam path. Scattering runs were also performed on the empty cans and spectrometer background in order to allow subtraction from the sample scattering data, and on a standard vanadium rod of the same size and shape as the cans. After standard corrections to the data for attenuation and multiple scattering of the neutron beam (Soper et al., 1989), the scattering from the sample container and spectrometer background were subtracted from the data, and division by the vanadium standard performed in order to express the scattering cross sections in absolute units. Corrections to the data for inelasticity effects were also performed, which finally yielded the total elastically scattered intensity for the sample.

The oscillatory component of the total scattering is known as the total structure factor $S(Q)$, where $Q = 4\pi \sin \theta/\lambda$ for neutrons with wavelength λ scattered by the sample to an angle conventionally denoted by 2θ. The total structure factor is related by Fourier inversion to the real space function $G(r)$, known as the (total) reduced radial distribution function:

$$G(r) - 1 = \frac{2}{\pi}\int_0^\infty Q[S(Q) - 1]\sin Qr\,dr. \qquad (1)$$

This function expresses the probability of locating an atom at a radial distance between r and $r + dr$ from an arbitrary-origin atom. Peaks in $G(r)$ therefore correspond to nonrandom atomic correlations, and in the range $0.1 < r < 0.3$ nm can be assigned to specific interatomic bonds. In the special case of a monatomic system, the first peak in $G(r)$ will represent the bond length, or nearest-neighbor distance, the second peak the second-neighbor distance, and so on. The area under the first peak in $G(r)$ gives a measure of the mean number of nearest neighbors, or the coordination number.

In practice, however, it is not possible to measure the scattering to higher values of Q than some value Q_{max}. As a result, the integral in Eq. 1 will have an upper limit of Q_{max}, which is equivalent to multiplying the integrand by a step function $M(Q)$, where

$$M(Q) = 1 \quad \text{for} \quad Q \le Q_{max}$$
$$= 0 \quad \text{for} \quad Q > Q_{max}. \qquad (2)$$

The effect of this is to produce a $G(r)$ that is convoluted with the cosine transform of $M(Q)$, the so-called peak function $P(r)$, given by

$$P(r) = \frac{1}{\pi}\int_0^\infty M(Q)\cos(Qr)\,dQ$$
$$= \frac{Q_{max}}{\pi}\frac{\sin(Q_{max}r)}{Q_{max}r}. \qquad (3)$$

This function has a strong oscillatory component over a considerable range in r on either side of the main central peak, and these oscillations are known as termination ripples.

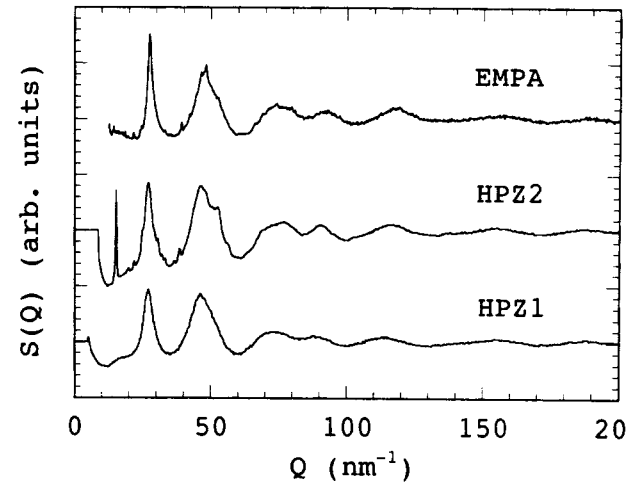

Figure 1. Structure factor S(Q) for the three amorphous fiber samples.

Curves are displaced vertically for clarity.

Results

The structure factor $S(Q)$ for each of the three samples is shown in Figure 1. In each case several broad peaks can be seen that are characteristic of amorphous materials. The strongest of these lie at approximately 27 nm^{-1} and 48 nm^{-1}, followed by weaker oscillations that are almost negligible in intensity after 200 nm^{-1} (the raw data extends as far as 500 nm^{-1}).

In the structure factor for HPZ2, however, an additional sharp peak is present at 15.2 nm^{-1}, which is a Bragg reflection from a crystalline component within the sample. Additional Bragg peaks, not visible in Figure 1, can also be seen in the uncorrected data for HPZ2 from individual detectors. Closer examination of the EMPA spectrum also reveals the presence of several Bragg peaks of low intensity, superimposed on the broader peaks in $S(Q)$. In the structure factor for HPZ1, the second peak is almost symmetrical, whereas in HPZ2—and to a lesser extent EMPA—this peak has a pronounced high-Q shoulder.

Each Bragg peak in $S(Q)$ can be related to an interplanar spacing d by the expression $d = 2\pi/Q_B$, where Q_B is the position of the Bragg peak. The values of d can then be checked against standard x-ray powder patterns to determine the crystalline phases present in the sample. The results for samples HPZ2 and EMPA are presented in Table 1 along with their respective assignments. While the crystalline inclusions in sample EMPA are purely α-Si_3N_4, sample HPZ2 appears to contain several crystalline phases. The d-spacing of 0.413

Table 1. Measured d-Spacings and Their Assignments for Bragg Peaks in Structure Factors for HPZ2 and EMPA

HPZ2		EMPA	
d (nm)	Phase	d (nm)	Phase
0.413	Cristobalite	0.338	α-Si_3N_4
0.314	Si	0.289	α-Si_3N_4
0.288	α-Si_3N_4	0.255	α-Si_3N_4
0.208	α-Si_3N_4	0.228	α-Si_3N_4
0.161	α-Si_3N_4	0.160	α-Si_3N_4

nm does not correspond to Si, SiC, or Si_3N_4, and on the basis of electronic microscopy analysis (described below) is assumed to correspond to cristobalite.

Since neutron scattering is a bulk method, it is impossible to determine whether amorphous and crystalline features in $S(Q)$ originate from distinct fibers or a single fiber. In order to further investigate the presence of crystallinity in samples HPZ2 and EMPA, transmission electron microscopy (TEM) analysis has been carried out using a JEOL 2010 microscope with a line resolution of approximately 0.14 nm. A small portion of the powdered samples used for neutron scattering measurements was suspended in acetone, from which a drop of the suspension was placed on a standard 3-mm copper grid covered with a perforated carbon film for insertion into the microscope.

In sample HPZ2, crystallites extremely sensitive to the electron beam were observed with d-spacings of 0.41 nm (Gilkes, unpublished work). These crystallites very quickly become amorphous producing only diffuse halos in the electron diffraction pattern. The spacing of 0.41 nm is close to that of the cristobalite phase (0.415 nm) observed in heat-treated Nicalon fibers (Maniette and Oberlin, 1989). Since the HPZ fibers are likely to possess an amorphous SiO_2 component, it is possible that this component crystallizes during annealing to form cristobalite particles.

TEM investigation of individual HPZ2 fibers reveals both amorphous and crystalline components. Figure 2 shows a high-magnification TEM image of the edge of a fiber particle, and crystallites of Si with 0.32-nm spacings can be seen embedded in the amorphous matrix. In the case of sample EMPA, however, TEM analysis reveals two distinct types of fiber particles. One is crystalline, with lattice spacings matching those of α-Si_3N_4, and the other amorphous (Gilkes, unpublished work). Very few particles exhibited diffraction patterns with both amorphous and crystalline features.

The reduced radial distribution functions $G(r)$ for each of the three samples has been obtained by Fourier inversion of the structure factors (Eq. 1), and these are shown in Figure 3. In each case, the main peak lies between 0.172 and 0.174 nm,

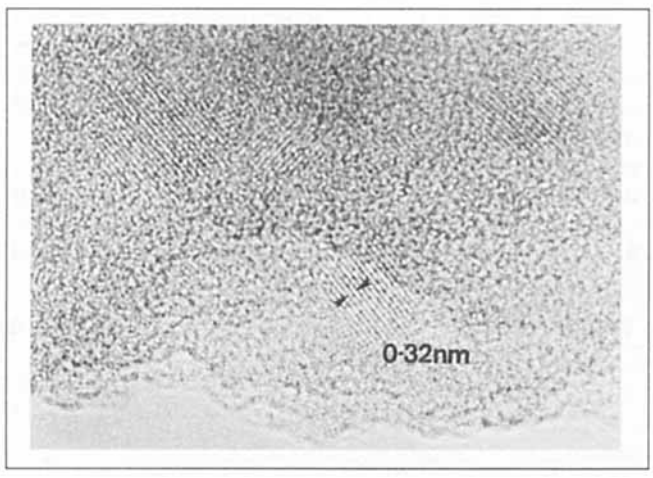

Figure 2. TEM bright-field image of part of a fiber from sample HPZ2.

It shows both amorphous and crystalline regions with 0.32-nm interplanar spacings.

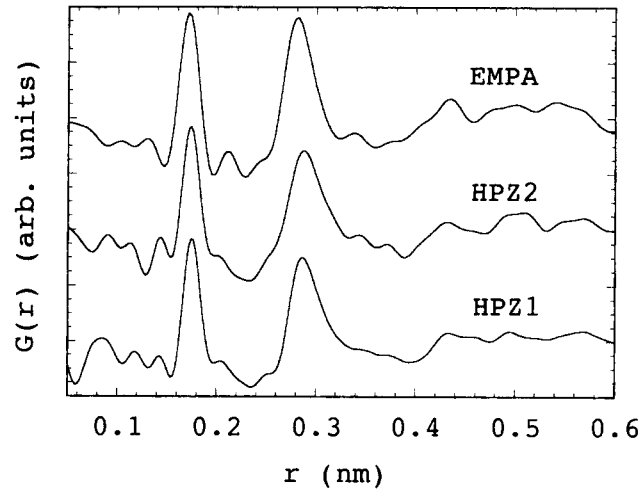

Figure 3. Reduced radial distribution function $G(r)$ for the three amorphous fiber samples.

Curves are displaced vertically for clarity.

which is close to the Si–N bond length in crystalline Si_3N_4 (0.173 nm). The second peak lies at about 0.280 nm. Other smaller peaks can be seen in the data, and while some of these may be structural in origin, several are artefacts produced by the truncation of the Q-space data. This effect is particularly noticeable for the first peak, which has equally spaced sidebands at 0.13 nm and 0.21 nm. These sidebands can be seen most clearly in the data for the EMPA sample.

The data for HPZ1 and HPZ2 do not possess clear symmetrical sidebands, but rather appear to possess an extra *structural* peak at 0.143 nm. This value is close to the C–C bond length in graphite (0.142 nm), confirming the presence of free carbon in both HPZ1 and HPZ2. Peaks in $G(r)$ below 0.12 nm are not viewed as structurally significant, as low-frequency oscillations in $S(Q)$—arising from the inability to adequately correct the data for inelastic scattering from small amounts of H in the sample—will give rise (through Eq. 1) to unphysical peaks in $G(r)$ at very low r-values.

Discussion

Ignoring for the moment the Bragg peaks in $S(Q)$, the curves in Figure 1 are closely similar to published data for thin-film a-Si_3N_4 produced by chemical vapor deposition (CVD) (Misawa et al., 1979). For this material, the second peak in $S(Q)$ is found to be symmetrical, suggesting that the Si_3N_4 component of HPZ1 comes closest to forming a truly amorphous network. The presence of a shoulder to this peak in the other samples—particularly the annealed HPZ2 sample—suggests that the structural ordering in the HPZ2 and EMPA samples is closer to crystalline α-Si_3N_4, as the structure factor for crystalline α-Si_3N_4 has a strong peak at 53 nm^{-1} (Gilkes, unpublished work). In the case of EMPA, the sample is composed of distinct amorphous and crystalline fibers, and if the latter were removed the structure factor would more closely resemble that of CVD a-Si_3N_4. On the other hand, TEM findings suggest that the HPZ2 sample contains fibers in which both crystalline and amorphous regions occur on a microscopic scale, possibly through growth of crystalline nuclei already present in the as-prepared fibers.

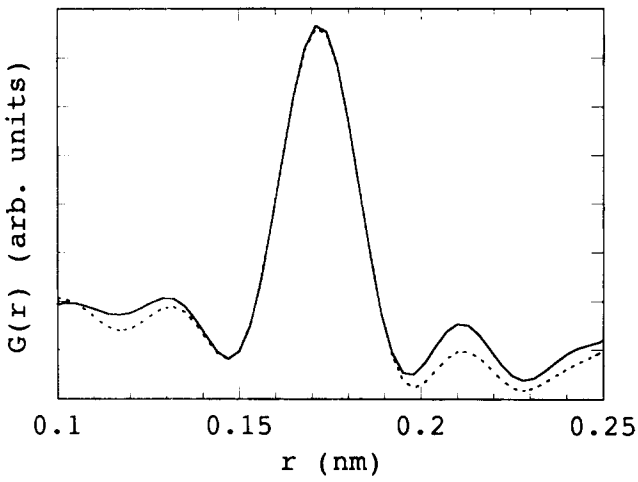

Figure 4. Gaussian fit (dotted) to the first peak in $G(r)$ (solid) for the EMPA fiber sample.

The real-space data of Figure 3 reveal the presence of graphitic carbon in both HPZ1 and HPZ2, as observed by other workers (Lipowitz, 1991). The carbon component in these fibers is likely to be disordered, as crystalline graphite produces a strong Bragg peak in $S(Q)$ at 18.8 nm^{-1}, and no such peak is present in Figure 1. In addition, no crystalline graphite was found during TEM analysis of the fibers. The position of the main peak in $G(r)$ around 0.173 nm is consistent with a material dominated by covalent Si–N bonding. If the second peak in $G(r)$ at about 0.28 nm is assumed to arise mainly from N–N second neighbors, the mean bond angle θ can easily be calculated using the expression $\theta = 2\ \sin^{-1}(R_2/2R_1)$, where R_1 and R_2 are the positions of the first and second peaks, respectively. This yields a value of approximately 111° for samples HPZ1 and HPZ2, and 110° for sample EMPA, all of which are close to the tetrahedral angle of 109.5°.

Although sample HPZ1 has a structure factor that most closely resembles that of CVD a-Si_3N_4, the atomic composition of sample EMPA is closest to that of pure Si_3N_4. No C–C bonds are present in $G(r)$ for this sample, and the first (Si–N) peak is almost perfectly symmetrical. A fit to the peaks in Figure 3 can be made by placing Gaussians at the correct positions in r-space and convoluting them with the appropriate peak function (Eq. 3) to simulate the effects of truncation of $S(Q)$. A fit to the first peak in $G(r)$ for EMPA has been made using a single Gaussian centered at 0.172 nm—this fit is shown in Figure 4. The fit can be seen to reproduce the experimental peak almost exactly, and reproduces correctly the positions of the two sidebands resulting from truncation of $S(Q)$.

This suggests that other bonds involving Si are unlikely to be present in significant proportions, such as Si–O bonds, which would occur at around 0.16 nm. This does not, however, rule out the possibility of the presence of an amorphous silicon oxynitride component with composition $Si_3N_{4-x}O_{1.5x}$, suggested by NMR measurements (Vogt et al., 1995), but implies that $x \ll 1$. More accurate measurements of the composition of the fibers are currently being made (Pillinger, work in progress), in order to allow a detailed analysis of the real-space data involving the extraction of the coordination numbers for each sample.

Conclusions

Neutron scattering measurements performed on three amorphous fibers reveal distinctive similarities and differences in their atomic structure. While the as-prepared fibers produced through pyrolysis of a polymer precursor have an amorphous structure closely similar to CVD-produced a-Si_3N_4, annealing at 1,400°C in N_2 for 100 h produces extensive crystallization of the residual polymeric component, and partial crystallization of the Si_3N_4 matrix. In addition, both samples possess excess disordered carbon.

The fibers grown by vapor deposition of ammonia on silica are also predominantly amorphous, but do contain a small proportion of crystalline α-Si_3N_4. It is possible that these inclusions result from temperature fluctuations within the deposition cell that favor growth of the crystalline material. The real-space data for these fibers show that the atomic structure of the material is close to pure Si_3N_4, with very little bonded oxygen present in the fiber matrix.

Acknowledgments

The author thanks Dow Corning and EMPA for providing the amorphous fibers used in this work, W. S. Howells and A. C. Hannon for assistance with the ISIS experiments, and D. Jefferson for use of the JEOL 2010 transmission electron microscope.

Literature Cited

Chollon, G., U. Vogt, and K. Berroth, "Thermal Behaviour of a Si-N-(O) Fiber," *Proc. ACERS*, Indianapolis, (1996).

Legrow, G. E., T. F. Lim, J. Lipowitz, and R. S. Reaoch, "Ceramics from Hydridopolysilazane," *Amer. Ceram. Soc. Bull.*, **66**(2), 363 (1987).

Lipowitz, J., "Polymer-Derived Ceramic Fibers," *Ceram. Bull.*, **70**(12), 1888 (1991).

Maniette, Y., and A. Oberlin, "TEM Characterisation of Some Crude or Air Heat-Treated SiC Nicalon Fibers," *J. Mater. Sci.*, **24**, 3361 (1989).

Misawa, M., T. Fukunaga, K. Nihara, and K. Suzuki, "Structure Characterisation of CVD Amorphous Si_3N_4 by Pulsed Neutron Total Scattering," *J. Non-Cryst. Solids*, **34**, 313 (1979).

Soper, A. K., W. S. Howells, and A. C. Hannon, *Rutherford Appleton Lab. Rep.*, RAL 89-046, Rutherford Laboratory, Oxfordshire, UK (1989).

Vogt, U., J. Kubler, and G. Engeli, "Silicon Nitride Fibers Synthesized by a Gas-Phase Process," *Proc. Cocoa Beach Conf.*, (1995).

Vogt, U., G. Chollon, and K. Berroth, "Synthesis, Composition and Ultra-High Temperature Characterization of Si-N-(O) Fibers and Initial Incorporation in CMCs," *Proc. Int. Symp. on Ultra-High Temperature Materials*, Tajimi, Japan (1996).

Manuscript received Oct. 28, 1996, and revision received Mar. 11, 1997.